Convergence of Convective Updraft Ensembles With Respect to the Grid Spacing of Atmospheric Models

Sueki, Kenta ; Yamaura, Tsuyoshi ; Yashiro, Hisashi ; Nishizawa, Seiya ; Yoshida, Ryuji ; Kajikawa, Yoshiyuki ; Tomita, Hirofumi

(Citation)
Geophysical Research Letters,46(24):14817-14825

(Issue Date)
2019-12-28

(Resource Type)
journal article

(Version)
Version of Record

(URL)
https://hdl.handle.net/20.500.14094/90007234

Geophysical Research Letters

RESEARCH LETTER
10.1029/2019GL084491

Convergence of Convective Updraft Ensembles With Respect to the Grid Spacing of Atmospheric Models

Kenta Sueki[1,2], Tsuyoshi Yamaura[1,3], Hisashi Yashiro[1,4], Seiya Nishizawa[1], Ryuji Yoshida[5,6], Yoshiyuki Kajikawa[1,3], and Hirofumi Tomita[1,2]

[1]RIKEN Center for Computational Science, Kobe, Japan, [2]RIKEN Cluster for Pioneering Research, Kobe, Japan, [3]Research Center for Urban Safety and Security, Kobe University, Kobe, Japan, [4]Now at National Institute for Environmental Studies, Tsukuba, Japan, [5]CIRES, University of Colorado Boulder, Boulder, CO, USA, [6]NOAA Earth System Research Laboratory, Boulder, CO, USA

Abstract Atmospheric deep moist convection can organize into cloud systems, which impact the Earth's climate significantly. High-resolution simulations that correctly reproduce organized cloud systems are necessary to understand the role of deep convection in the Earth's climate system. However, there remain issues regarding convergence with respect to grid spacing. To investigate the resolution necessary for a reasonable simulation of deep convection, we conducted grid-refinement experiments using state-of-the-art atmospheric models. We found that the structure of an updraft ensemble in an organized cloud system converges at progressively smaller scales as the grid spacing is reduced. The gap between two adjacent updrafts converges to a particular distance when the grid spacing becomes as small as 1/20–1/40 of the updraft radius. We also found that the converged inter-updraft distance value is not significantly different between Reynolds-averaged Navier–Stokes simulations and large eddy simulations for grid spacings in the terra incognita range.

Plain Language Summary Meteorologists use computer simulations to predict atmospheric phenomena. When simulating the atmosphere, they divide it into small boxes and calculate the changes in wind speed, amounts of moisture and precipitation, and other important variables in each box. Here, our question is how finely we should divide the atmosphere to obtain the correct "answer" in the simulations; we call this *the convergence problem*. The more finely we divide the atmosphere, the more closely the simulation results approach the correct answer, but the more computational resources we need. The convergence problem is an important topic for us when carrying out accurate atmospheric simulations with limited computational power. This paper has addressed this problem. The target of our simulation is a group of cumulonimbus clouds. We performed several simulations with progressively smaller boxes to investigate how finely we should divide the atmosphere to reach convergence. We found that we should divide the atmosphere so that the width of each box is as small as 1/20 to 1/40 of the width of an upward current in an individual cumulonimbus cloud. We believe that this paper provides a new guideline for accurate atmospheric simulations.

Key Points:
- We conducted grid refinement experiments with convection-permitting atmospheric models to assess convergence of deep convective updrafts
- The experiments reveal that the statistics of convective updrafts in organized cloud systems converge at progressively smaller scales
- Reynolds-averaged Navier–Stokes simulations and large eddy simulations reach almost the same converged structure

Supporting Information:
- Supporting Information S1

Correspondence to:
K. Sueki,
kenta.sueki@riken.jp

Citation:
Sueki, K., Yamaura, T., Yashiro, H., Nishizawa, S., Yoshida, R., Kajikawa, Y., & Tomita, H. (2019). Convergence of convective updraft ensembles with respect to the grid spacing of atmospheric models. *Geophysical Research Letters*, *46*, 14,817–14,825. https://doi.org/10.1029/2019GL084491

Received 10 JUL 2019
Accepted 21 NOV 2019
Accepted article online 4 DEC 2019
Published online 17 DEC 2019

1. Introduction

Deep convective clouds in the atmosphere have a major impact on climate sensitivity (Bony et al., 2015). However, there are still issues with their representation in climate models, causing great uncertainty in climate prediction (Mauritsen & Stevens, 2015; Stevens & Bony, 2013). Convective clouds often form self-organized systems with spatially hierarchical structures, such as tropical cyclones or super cloud clusters associated with Madden–Julian oscillations (MJO; Madden & Julian, 1972). This self-organization of convective clouds makes it difficult to assess their impact on the climate (Bony et al., 2015; Mauritsen & Stevens, 2015). For a better understanding of the behavior of cloud systems and their roles in the global circulation, numerical models that can simulate cloud systems from the elementary processes of atmospheric convection (i.e., cloud microphysics and turbulence) are useful tools. However, the convergence with respect to grid spacing remains debated. Here, convergence is defined as the state in which the structure of the simulated deep convection does not substantially change with further grid-spacing reductions.

Previous studies have shown that at least a 4-km horizontal grid spacing is necessary to simulate the structure of deep convective systems plausibly (Weisman et al., 1997), a 250-m grid spacing is required to resolve

isotropic turbulent flow in deep convection (Bryan et al., 2003), and a 200-m grid spacing is needed to achieve convergence for the vertical velocity profiles in deep convective updrafts (Khairoutdinov et al., 2009). Large scale heating and moistening due to deep moist convection are known to converge at around a 1-km grid spacing both for idealized (Panosetti et al., 2018) and real cases with complex terrains (Langhans et al., 2012; Panosetti et al., 2019). The convergence of large-scale tendencies is referred to as "bulk convergence" (Langhans et al., 2012), the achievement of which implies climate simulation capability of convection-permitting models with kilometer-scale grid spacing. On the other hand, "structural convergence," defined as the convergence of the statistics of individual cloud-scale structures (Panosetti et al., 2018), is known to not have been achieved even at a subkilometer grid spacing. Miyamoto et al. (2013, 2015) investigated the grid-spacing dependence of the distance between the updraft cores of deep moist convection in a global model; however, convergence was not obtained even at an 870-m grid spacing. Panosetti et al. (2018, 2019) showed that a 550-m grid spacing is insufficient for the structural convergence of deep convection, unlike the bulk convergence. Parameter tuning of coarse-resolution models whose convergence is achieved only in the bulk sense does not guarantee the predictability of unknown future climate change. Comparing a converged structure of organized cloud systems with its natural counterpart is fundamental for improving their representation in our state-of-the-art atmospheric models. In this sense, the structural convergence of deep convection is important not only for short-term weather prediction, focusing on cloud-scale phenomena such as localized heavy rainfall and severe winds, but also for constructing reliable climate models.

We explored the structural convergence of deep convection by systematically performing grid refinement experiments. We focused on convective updraft as in our previous studies (Miyamoto et al., 2013, 2015). Jeevanjee (2017) showed that the average vertical velocity of convective parcels converges at a 250-m grid spacing, while the average parcels' aspect ratio does not converge even at sub-100-m grid spacing; that is, the convergence of deep convective updraft is achieved in the bulk sense but not in the structural sense. This paper shows that the simulated convective system contains updraft ensembles with multiple-scale structures and converges at progressively smaller scales as grid spacing is reduced.

2. Methods

2.1. Experimental design

The simulation target was deep convection associated with the MJO in late November 2011. This was a typical MJO event observed during the CINDY2011/DYNAMO international field campaign (Yoneyama et al., 2013). See Figure 1 for an overview of experimental design and the sequence of procedures. First, we conducted global simulations with a horizontal grid spacing of 3.5 km using the Nonhydrostatic ICosahedral Atmospheric Model (NICAM; Tomita & Satoh, 2004; see also Satoh et al., 2014), which has been shown to yield realistic MJO simulations (Miura et al., 2007; Miyakawa et al., 2014). The initial conditions were constructed from the final operational global analysis data at 00:00 UTC on 21 November 2011, provided by the National Centers for Environmental Prediction. Next, an active convective region was downscaled using the Scalable Computing for Advanced Library and Environment-Regional Model (SCALE-RM; Nishizawa et al., 2015; Sato et al., 2015; Yoshida et al., 2017). In the downscaling experiments, we performed two series of experiments using one-way online nesting systems: a coarse-resolution experiment with grid spacings from 3,200 to 200 m (Exp-A), and a fine-resolution experiment with grid spacings from 800 to 50 m (Exp-B). The initial and boundary conditions of Exp-A were constructed from the NICAM output and those of Exp-B from the output of Exp-A with 800-m grid spacing.

2.2. Model Physics

In the NICAM simulation, microphysical processes, boundary layer turbulence effects, and radiation effects were parameterized using a six-class single-moment scheme (Tomita, 2008), Level 2 closure of the improved Mellor–Yamada scheme (Mellor–Yamada–Nakanishi–Niino [MYNN] scheme; Nakanishi & Niino, 2004, 2006), and mstrnX scheme (Sekiguchi & Nakajima, 2008), respectively. In Exp-A and Exp-B by SCALE-RM, the same microphysics and radiation schemes as in the NICAM simulation were used. Except for the grid spacing, domain size, and simulated time, the main difference between Exp-A and Exp-B was in the representation of the subgrid scale (SGS) turbulence. In Exp-A, a Level 2.5 closure of the MYNN scheme, which is based on a prognostic equation for turbulent kinetic energy, was used, whereas the

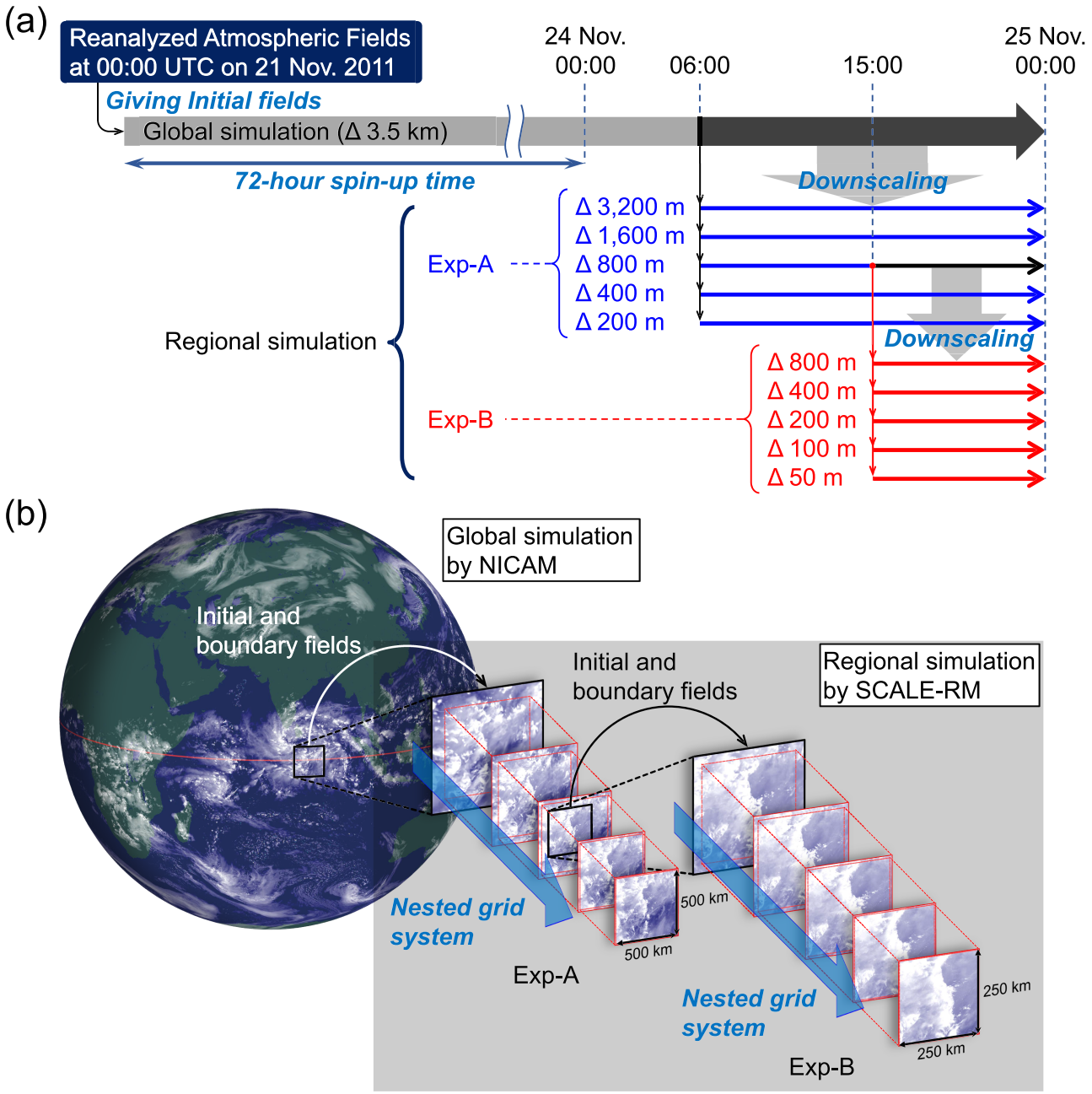

Figure 1. Experimental schematic. (a) Experimental outline. The time is expressed in universal time coordinated (UTC). (b) Snapshots of the total column condensate for each simulation at 18:00 UTC on 24 November 2011.

Smagorinsky-type scheme (Brown et al., 1994; Lilly, 1962; Scotti et al., 1993; Smagorinsky, 1963) was used in Exp-B. The MYNN scheme is based on the Reynolds-averaged Navier–Stokes equations which is usually applied to horizontal grid spacings of more than 1 km and only calculates the SGS turbulent mixing in the vertical direction. That is, the horizontal diffusion is not explicitly treated in Exp-A. On the other hand, the Smagorinsky scheme is used for a large eddy simulation with sub-100-m grid spacing and calculates SGS turbulent mixing in three dimensions. SGS turbulence parameterization for intermediate grid spacing has been referred to as a "terra incognita" (Wyngaard, 2004) and remains a controversial issue in the modeling community (e.g., Honnert et al., 2016; Ito et al., 2015; Kitamura, 2016; Shin & Hong, 2015). Our experiments applied both the MYNN and Smagorinsky schemes to the grid spacing in

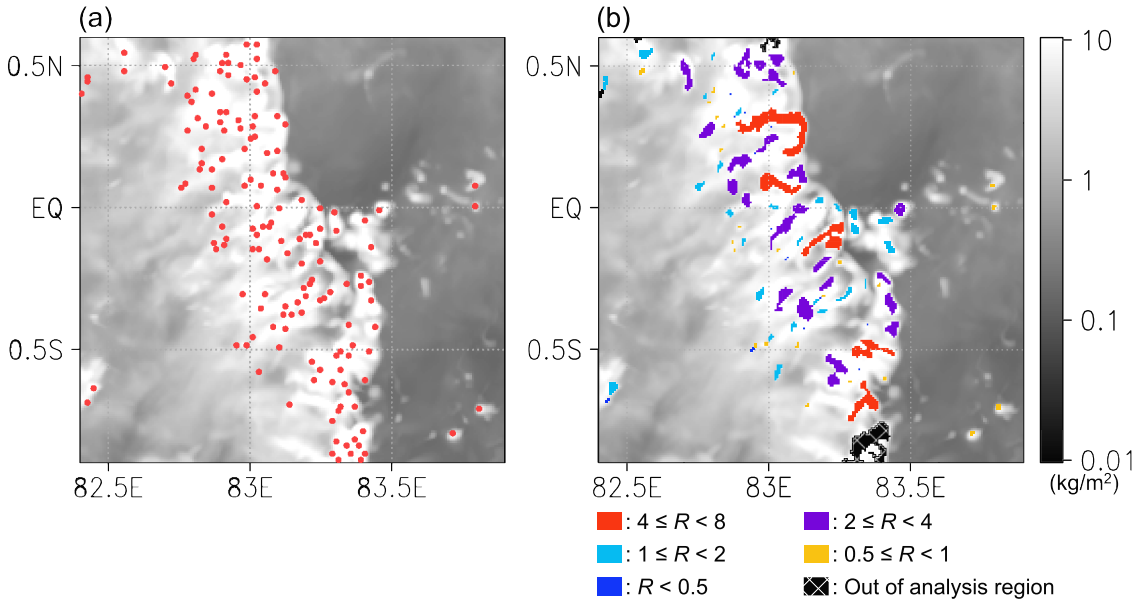

Figure 2. Example of updraft cores detected by the two different algorithms. (a) Updraft cores detected by Algorithm 1 (red dots). (b) Updraft cores detected by Algorithm 2 (colored objects). In (b), different colors indicate different size classifications: Each updraft core is classified by its effective radius, R (unit: km), which is defined as the square root of area S divided by π: $R \equiv (S/\pi)^{1/2}$. If part of the updraft core protruded from the analysis region, it was removed from the statistical analysis (objects shown by black and white check pattern). Both panels show snapshots of the total column condensate (kg/m^2) at 1750 UTC for Exp-B with 800-m grid spacing.

the terra incognita range (800, 400, and 200 m) to check the differences in their convergence behavior. Detailed model configurations are listed in Tables S1 and S2 in the supporting information.

2.3. Algorithms for Detecting Deep Convective Updraft Cores

Our study used two different algorithms to detect separate deep convective updrafts. The first algorithm (Algorithm 1) is similar to the procedure used in our previous studies (Miyamoto et al., 2013, 2015). First, deep cloud regions are determined using the ISCCP simulator (Klein & Jakob, 1999; Webb et al., 2001), a satellite simulator for estimating the optical thickness, τ, and cloud top pressure, p_{top}, of model columns. In this study, deep cloud regions were defined as regions where $\tau \geq 60$ and $p_{\mathrm{top}} < 440$ hPa. Next, the vertically averaged vertical velocity from the surface to the cloud top ($\overline{w}^{\mathrm{cloud}}$) was calculated in the deep cloud regions, where the cloud top was defined as the uppermost model level whose optical thickness from the model top is larger than 0.1. Finally, each updraft core is defined as a local $\overline{w}^{\mathrm{cloud}}$ maximum with the provision that $\overline{w}^{\mathrm{cloud}}$ is equal to or larger than a particular threshold value, $\overline{w}_0$. In the second algorithm (Algorithm 2), each updraft core is defined as a continuous region where $\overline{w}^{\mathrm{cloud}}$ is equal to or larger than the same $\overline{w}_0$ used in Algorithm 1. The central position of each updraft core was defined as the "center of gravity" of $\overline{w}^{\mathrm{cloud}}$ and used to calculate the distance between updraft cores. Schematic illustrations of the two algorithms are shown in Figure S1. The threshold value, $\overline{w}_0$, was set to 0.5 m/s so that the mean vertical velocity profiles at the outer edges of updraft cores reach at least 1 m/s in the middle of the troposphere (see Text S1 and Figure S2 in the supporting information). Figure 2 shows an example of updraft cores extracted from a simulation snapshot. Although the updraft cores detected by Algorithm 1 are just points (Figure 2a), those detected by Algorithm 2 are two-dimensional objects; therefore, each core has a different area (Figure 2b). These two types of updraft core are qualitatively different. Therefore, the convergence behavior is also expected to be different.

3. Results

3.1. Results Obtained Using Algorithm 1

Figure 3 shows the grid-spacing dependence of the updraft cores detected by Algorithm 1, including the number of updraft cores per 10,000 km^2 deep cloud region (Figure 3a) and the mean value of the

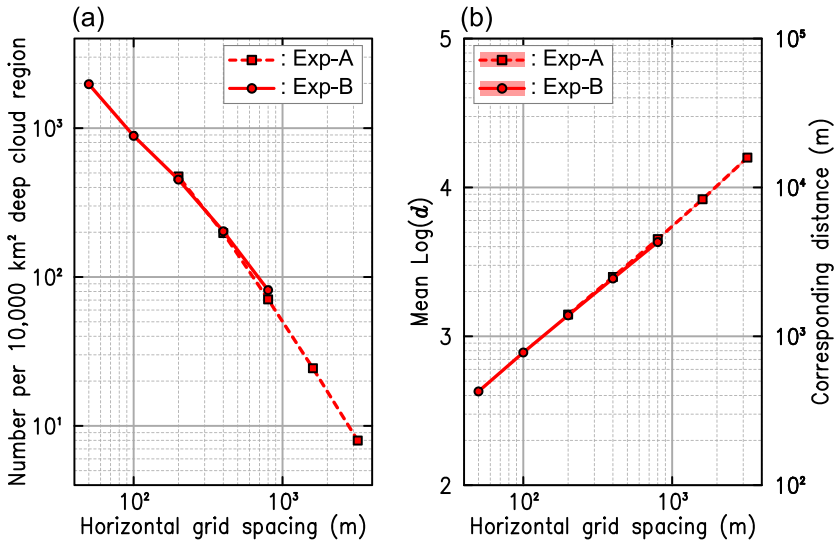

Figure 3. Horizontal grid-spacing dependence of updraft cores detected by Algorithm 1. (a) Number of updraft cores per 10,000 km^2 deep cloud region. (b) Mean value of the logarithm of the distance, d, between nearest-neighbor two cores, denoted by mean Log(d). The dashed and solid lines indicate Exp-A and Exp-B, respectively. In (b), a confidence interval of 99% for mean Log(d) is indicated by the translucent color. In this study, the confidence interval was calculated under the assumption that the population of Log(d) follows the normal distribution. However, the confidence interval cannot be seen clearly in this figure because it is narrow.

logarithm of the distance, d, between two nearest-neighbor cores, denoted by mean Log(d) (Figure 3b). The logarithm of d was used because its distribution has a strong positive skewness (Figure S3). We found that the number density of the cores continued to increase up to a 50-m grid spacing (Figure 3a), that is, convergence for the updraft cores was not achieved when we reduced the grid spacing further than in our previous studies (Miyamoto et al., 2013, 2015). The mean Log(d) also showed no convergence (Figure 3b). The corresponding distance for mean Log(d) gradually increases from 5 to 8.5 times the grid spacing as the resolution increases. The intervals of adjacent updraft cores detected by Algorithm 1 are close to the scale of the so-called "effective resolution" (7 times the grid spacing) where the kinetic energy spectrum falls off the −5/3 slope in numerical atmospheric simulations (Skamarock, 2004). Algorithm 1 probably detects all the small structures with a size below the physically meaningful updraft structure. Therefore, the distance will not converge as long as we use this algorithm. Interestingly, the mean Log(d) for Exp-A and Exp-B are almost indistinguishable for grid spacings between 800 and 200 m, although Exp-A is less diffusive because of the absence of horizontal SGS turbulent mixing (see section 2.2).

3.2. Results Obtained Using Algorithm 2

Unlike Algorithm 1, Algorithm 2 provides information about the two-dimensional size of each detected updraft core. Figure 4 shows the data obtained using Algorithm 2, similarly to Figure 3. In Figure 4, the statistics for different size categories are shown. Each updraft core is categorized by its effective radius, R, which is defined as the square root of area S divided by π: $R \equiv (S/\pi)^{1/2}$. We removed the updraft cores with $R \geq 8$ km from the analysis because their sample size is too small for statistical analysis. Figure 4a shows that the number density for each size category reaches its maximum at different grid spacings, except for $R < 0.5$ km. We found that the maximum point scales perfectly with the effective radius of each size category: those for R = 4–8, 2–4, 1–2, and 0.5–1 km are located at grid spacings of 1,600, 800, 400, and 200 m, respectively. Figure 4b shows that the variation in mean Log(d) with respect to the grid spacing also scales with the effective radius. The minima of mean Log(d) for R = 4–8, 2–4, 1–2, and 0.5–1 km are located at grid spacings of 800, 400, 200, and 100 m, respectively. At the minimum, the horizontal scale of the updraft core corresponds to the effective resolution of the model: R is 5–10 times as large as the grid spacing. The mean Log(d) increases as the grid spacing is further reduced from the minimum point, indicating that the minimum is not the convergence point. For R = 4–8 and 2–4 km, convergence seems to occur at 200- and 100-m grid spacings, respectively. Therefore, a grid spacing as small as 1/20–1/40 of R is required for convergence. This

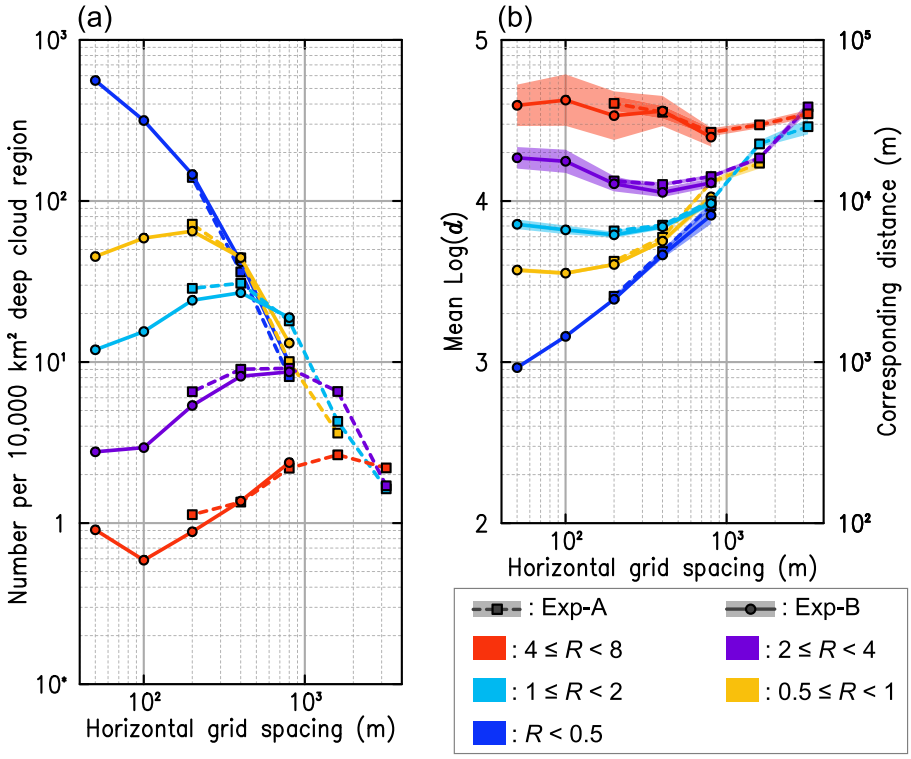

Figure 4. Horizontal grid-spacing dependence of updraft cores detected by Algorithm 2. (a) Number of updraft cores per 10,000 km^2 deep cloud region. (b) Mean value of the logarithm of the distance, d, between nearest-neighbor two cores, denoted by mean Log(d). The dashed and solid lines indicate Exp-A and Exp-B, respectively. Different colors indicate different size classifications. In (b), a confidence interval of 99% for mean Log(d) is indicated by the translucent color.

conclusion is also supported by the convergence of the kinetic energy power spectral density. The converged mean Log(d) value for R = 4–8 km (2–4 km) corresponds to a distance of about 40 km (20 km; Figure 4b), while the power spectral density corresponding to a wavelength of 40 km (20 km) for a height of about 8 km sufficiently converges at a grid spacing of 400 m (200 m; see Text S2 and Figure S4). Assuming a simple scaling law, we can speculate that mean Log(d) for R = 1–2 km and 0.5–1 km will converge at grid spacings of 50 m and 25 m, respectively. As with the number density, the smallest category (R < 0.5 km) does not reach the minimum. However, the minimum and convergence points can be estimated from the above scaling law if it is further classified into R = 250–500 m, 125–250 m, and so on. We conclude that the structure of updraft ensemble in deep moist convection converges at progressively smaller scales in accordance with the scaling law with respect to the horizontal scale of the convective updraft.

4. Discussion

For the results of both algorithms, the mean Log(d) values for Exp-A and Exp-B are not significantly different in the terra incognita range. In the case of the updraft core of R = 4–8 km detected by Algorithm 2, the confidence intervals of 99% for Exp-A and Exp-B overlap from the minimum point (800-m grid spacing) to the convergence point (200-m grid spacing; Figure 4b). In the simulations, horizontal diffusion by the SGS turbulence model acted only in Exp-B. By contrast, the implicit numerical diffusion associated with the advection scheme acted in both Exp-A and Exp-B because we used third-order upwind spatial discretization (Table S2). If the implicit numerical diffusivity rather than the SGS turbulent diffusivity was dominant in the terra incognita range, a comparison of Exp-A and Exp-B would be meaningless. To assess this concern, we compared the impacts of implicit numerical diffusion and SGS turbulent diffusion using a simple scale analysis. According to Nishizawa et al. (2015), the time scale of implicit numerical diffusion, T_{num}, for the third-order upwind spatial discretization can be estimated as $T_{num} \sim 12L^4/U\Delta x^3$, where L is the horizontal scale of variation, U is the wind speed, and Δx is the grid spacing. Meanwhile, the time scale of SGS turbulent

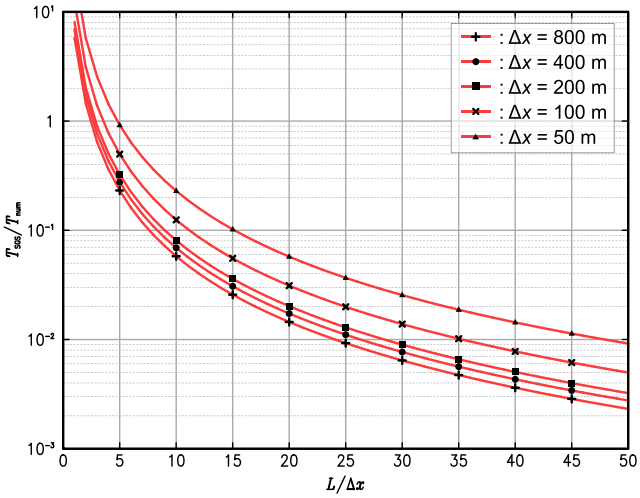

Figure 5. The ratio of the time scale of SGS turbulent diffusion (T_{SGS}) to the time scale of implicit numerical diffusion (T_{num}). The x axis shows the horizontal scale of variation L normalized by the grid spacing, Δx. Different marks indicate different grid spacings for Exp-B.

diffusion, T_{SGS}, can be estimated as $T_{SGS} \sim L^2/\nu_{SGS}$, where ν_{SGS} is the coefficient of eddy viscosity. Thus, the ratio of T_{SGS} to T_{num} becomes

$$\frac{T_{SGS}}{T_{num}} \sim \frac{U}{12}\frac{\Delta x}{\nu_{SGS}}\left(\frac{\Delta x}{L}\right)^2 \quad (1)$$

Figure 5 shows the change in T_{SGS}/T_{num} with respect to the horizontal scale of variation L. We assumed $U = 10$ m s^{-1} and used the median ν_{SGS} of the whole analysis domain and period to estimate Equation (1). Note that the SGS turbulence model used in this study acts only when the pointwise Richardson number, Ri, is less than 0.25, and thus, we considered only the grid satisfying Ri < 0.25 for the determination of the median ν_{SGS}. If the horizontal scale of variation is larger than the effective resolution ($L \approx 10\Delta x$), $T_{SGS}/T_{num} \ll 1$ (Figure 5). In this case, the time scale of diffusion by SGS turbulence is much shorter than that of the numerical viscosity, and thus, the impact of SGS turbulent diffusion is much larger than that of implicit numerical diffusion. For the convergence point of the updraft core with $R = 4$–8 km, where R is 20–40 times as large as the grid spacing (Figure 4b), we can conclude that the converged updraft structures are not significantly different between models with the MYNN and Smagorinsky schemes despite their different horizontal diffusivities. Therefore, the MYNN scheme can be used beyond the theoretically applicable range, provided that the focus is on the spatial arrangement of convective updrafts having a horizontal scale of around 4 km or larger. However, differences in the turbulence parameterization probably change the vertical moisture flux within the planetary boundary layer and, consequently, change the total area of the convective region. This issue will be addressed in our next study.

5. Conclusions and Remarks

We conducted grid-refinement experiments on the simulation of deep moist convection associated with an MJO event to investigate the structural convergence of a convective updraft ensemble in an organized cloud system. We clarified that the structure of an organized cloud system reaches convergence at progressively smaller scales. A grid spacing as small as 1/20–1/40 of the updraft effective radius is required for the statistical properties of convective updrafts converging. We conducted both Reynolds-averaged Navier–Stokes simulations and large eddy simulations using the MYNN and Smagorinsky schemes, respectively, finding a not significantly different convergence behavior. Thus, the MYNN scheme can be applied to grid spacing in the terra incognita range if we focus on the spatial arrangement of convective updrafts having a horizontal scale of several kilometers.

Our results yield guidelines for the required horizontal grid spacing by comparing simulated convection structures with a particular spatial scale in the current model to their counterparts in nature. The same procedure can be applied to other model frameworks, for example, different microphysics and turbulence parameterizations, and other types of organized cloud systems, such as tropical cyclones. The scaling law with respect to the effective radius offers hope for the construction of new statistical models for the hierarchical structure of organized cloud systems. The nature of organized cloud systems could be captured by satellite, for example, Tropical Rainfall Measuring Mission (Huffman et al., 2007) and Global Precipitation Measurement (Hou et al., 2014), ground-based weather radar, and aircraft observation (e.g., LeMone & Zipser, 1980). Comparing these observations with high-resolution simulations could lead to improving numerical atmospheric models, which are required for understanding the essential role of deep moist convection.

Acknowledgments
We thank the three anonymous reviewers of our manuscript for their helpful suggestions. This work was supported by JST CREST (Grant JPMJCR1312), Japan. This research used computational resources of the K computer provided by the RIKEN Center for Computational Science (RIKEN R-CCS) through the HPCI System Research project (Project ID: hp170113 and hp170232). We thank Editage (www.editage.jp) for their English language editing service. The figures were produced using GrADS (http://cola.gmu.edu/grads/). The NCEP FNL data is available at this site (https://doi.org/10.5065/D6M043C6). The code for NICAM version 15 can be provided from the NICAM development team (http://www.nicam.jp/). The code for SCALE-RM version 5.2.5 is freely available at http://r-ccs-climate.riken.jp/scale/download/index.html under the 2-Clause BSD license. All simulation data calculated by NICAM and SCALE-RM are deposited in the local storage at RIKEN R-CCS. Data, analysis codes, and model configuration files for NICAM and SCALE-RM, used for this study, are publicly available from Zenodo repository (https://doi.org/10.5281/zenodo.3543914).

References

Bony, S., Stevens, B., Frierson, D. M. W., Jakob, C., Kageyama, M., Pincus, R., et al. (2015). Clouds, circulation and climate sensitivity. *Nature Geoscience*, *8*(4), 261–268. https://doi.org/10.1038/ngeo2398

Brown, A. R., Derbyshire, S. H., & Mason, P. J. (1994). Large-eddy simulation of stable atmospheric boundary layers with a revised stochastic subgrid model. *Quarterly Journal of the Royal Meteorological Society*, *120*(520), 1485–1512. https://doi.org/10.1002/qj.49712052004

Bryan, G. H., Wyngaard, J. C., & Fritsch, J. M. (2003). Resolution requirements for the simulation of deep moist convection. *Monthly Weather Review*, *131*(10), 2394–2416. https://doi.org/10.1175/1520-0493(2003)131<2394:RRFTSO>2.0.CO;2

Honnert, R., Couvreux, F., Masson, V., & Lancz, D. (2016). Sampling the structure of convective turbulence and implications for grey-zone parameterizations. *Boundary-Layer Meteorology*, *160*(1), 133–156. https://doi.org/10.1007/s10546-016-0130-4

Hou, A. Y., Kakar, R. K., Neeck, S., Azarbarzin, A. A., Kummerow, C. D., Kojima, M., et al. (2014). The global precipitation measurement mission. *Bulletin of the American Meteorological Society*, *95*(5), 701–722. https://doi.org/10.1175/BAMS-D-13-00164.1

Huffman, G. J., Adler, R. F., Bolvin, D. T., Gu, G., Nelkin, E. J., Bowman, K. P., et al. (2007). The TRMM multisatellite precipitation analysis (TMPA): Quasi-global, multiyear, combined-sensor precipitation estimates at fine scales. *Journal of Hydrometeorology*, *8*(1), 38–55. https://doi.org/10.1175/JHM560.1

Ito, J., Niino, H., Nakanishi, M., & Moeng, C.-H. (2015). An extension of the Mellor–Yamada model to the terra incognita zone for dry convective mixed layers in the free convection regime. *Boundary-Layer Meteorology*, *157*(1), 23–43. https://doi.org/10.1007/s10546-015-0045-5

Jeevanjee, N. (2017). Vertical velocity in the gray zone. *Journal of Advances in Modeling Earth Systems*, *9*(6), 2304–2316. https://doi.org/10.1002/2017MS001059

Khairoutdinov, M. F., Krueger, S. K., Moeng, C.-H., Bogenschutz, P. A., & Randall, D. A. (2009). Large-eddy simulation of maritime deep tropical convection. *Journal of Advances in Modeling Earth Systems*, *1*(4), 15. https://doi.org/10.3894/JAMES.2009.1.15

Kitamura, Y. (2016). Improving a turbulence scheme for the terra incognita in a dry convective boundary layer. *Journal of the Meteorological Society of Japan, Series II*, *94*(6), 491–506. https://doi.org/10.2151/jmsj.2016-028

Klein, S. A., & Jakob, C. (1999). Validation and sensitivities of frontal clouds simulated by the ECMWF model. *Monthly Weather Review*, *127*(10), 2514–2531. https://doi.org/10.1175/1520-0493(1999)127<2514:VASOFC>2.0.CO;2

Langhans, W., Schmidle, J., & Schär, C. (2012). Bulk convergence of cloud-resolving simulations of moist convection over complex terrain. *Journal of the Atmospheric Sciences*, *69*(7), 2207–2228. https://doi.org/10.1175/JAS-D-11-0252.1

LeMone, M. A., & Zipser, E. J. (1980). Cumulonimbus vertical velocity events in GATE. Part I: Diameter, intensity and mass flux. *Journal of the Atmospheric Sciences*, *37*(11), 2444–2457. https://doi.org/10.1175/1520-0469(1980)037<2444:CVVEIG>2.0.CO;2

Lilly, D. K. (1962). On the numerical simulation of buoyant convection. *Tellus*, *14*(2), 148–171. https://doi.org/10.3402/tellusa.v14i2.9537

Madden, R. A., & Julian, P. R. (1972). Description of global-scale circulation cells in the tropics with a 40–50 day period. *Journal of the Atmospheric Sciences*, *29*(6), 1109–1123. https://doi.org/10.1175/1520-0469(1972)029<1109:DOGSCC>2.0.CO;2

Mauritsen, T., & Stevens, B. (2015). Missing iris effect as a possible cause of muted hydrological change and high climate sensitivity in models. *Nature Geoscience*, *8*(5), 346–351. https://doi.org/10.1038/ngeo2414

Miura, H., Satoh, M., Nasuno, T., Noda, A. T., & Oouchi, K. (2007). A Madden–Julian oscillation event realistically simulated by a global cloud-resolving model. *Science*, *318*(5857), 1763–1765. https://doi.org/10.1126/science.1148443

Miyakawa, T., Satoh, M., Miura, H., Tomita, H., Yashiro, H., Noda, A. T., et al. (2014). Madden–Julian oscillation prediction skill of a new-generation global model demonstrated using a supercomputer. *Nature Communications*, *5*, 3769. https://doi.org/10.1038/ncomms4769

Miyamoto, Y., Kajikawa, Y., Yoshida, R., Yamaura, T., Yashiro, H., & Tomita, H. (2013). Deep moist atmospheric convection in a subkilometer global simulation. *Geophysical Research Letters*, *40*, 4922–4926. https://doi.org/10.1002/grl.50944

Miyamoto, Y., Yoshida, R., Yamaura, T., Yashiro, H., Tomita, H., & Kajikawa, Y. (2015). Does convection vary in different cloud disturbances? *Atmospheric Science Letters*, *16*(3), 305–309. https://doi.org/10.1002/asl2.558

Nakanishi, M., & Niino, H. (2004). An improved Mellor–Yamada level-3 model with condensation physics: Its design and verification. *Boundary-Layer Meteorology*, *112*(1), 1–31. https://doi.org/10.1023/B:BOUN.0000020164.04146.98

Nakanishi, M., & Niino, H. (2006). An improved Mellor–Yamada level-3 model: Its numerical stability and application to a regional prediction of advection fog. *Boundary-Layer Meteorology*, *119*(2), 397–407. https://doi.org/10.1007/s10546-005-9030-8

Nishizawa, S., Yashiro, H., Sato, Y., Miyamoto, Y., & Tomita, H. (2015). Influence of grid aspect ratio on planetary boundary layer turbulence in large-eddy simulations. *Geoscientific Model Development*, *8*(10), 3393–3419. https://doi.org/10.5194/gmd-8-3393-2015

Panosetti, D., Schlemmer, L., & Schär, C. (2018). Convergence behavior of idealized convection-resolving simulations of summertime deep moist convection over land. *Climate Dynamics*, 1–20. https://doi.org/10.1007/s00382-018-4229-9

Panosetti, D., Schlemmer, L., & Schär, C. (2019). Bulk and structural convergence at convection-resolving scales in real-case simulations of summertime moist convection over land. *Quarterly Journal of the Royal Meteorological Society*, *145*(721), 1427–1443. https://doi.org/10.1002/qj.3502

Sato, Y., Nishizawa, S., Yashiro, H., Miyamoto, Y., Kajikawa, Y., & Tomita, H. (2015). Impacts of cloud microphysics on trade wind cumulus: Which cloud microphysics processes contribute to the diversity in a large eddy simulation? *Progress in Earth and Planetary Science*, *2*(1), 23. https://doi.org/10.1186/s40645-015-0053-6

Satoh, M., Tomita, H., Yashiro, H., Miura, H., Kodama, C., Seiki, T., et al. (2014). The non-hydrostatic icosahedral atmospheric model: Description and development. *Progress in Earth and Planetary Science*, *1*(1), 18. https://doi.org/10.1186/s40645-014-0018-1

Scotti, A., Meneveau, C., & Lilly, D. K. (1993). Generalized Smagorinsky model for anisotropic grids. *Physics of Fluids A: Fluid Dynamics*, *5*(9), 2306–2308. https://doi.org/10.1063/1.858537

Sekiguchi, M., & Nakajima, T. (2008). A k-distribution-based radiation code and its computational optimization for an atmospheric general circulation model. *Journal of Quantitative Spectroscopy and Radiative Transfer*, *109*(17–18), 2779–2793. https://doi.org/10.1016/j.jqsrt.2008.07.013

Shin, H. H., & Hong, S.-Y. (2015). Representation of the subgrid-scale turbulent transport in convective boundary layers at gray-zone resolutions. *Monthly Weather Review*, *143*(1), 250–271. https://doi.org/10.1175/MWR-D-14-00116.1

Skamarock, W. C. (2004). Evaluating mesoscale NWP models using kinetic energy spectra. *Monthly Weather Review*, *132*(12), 3019–3032. https://doi.org/10.1175/MWR2830.1

Smagorinsky, J. (1963). General circulation experiments with the primitive equations. *Monthly Weather Review*, *91*(3), 99–164. https://doi.org/10.1175/1520-0493(1963)091<0099:GCEWTP>2.3.CO;2

Stevens, B., & Bony, S. (2013). What are climate models missing? *Science*, *340*(6136), 1053–1054. https://doi.org/10.1126/science.1237554

Tomita, H. (2008). New microphysical schemes with five and six categories by diagnostic generation of cloud ice. *Journal of the Meteorological Society of Japan, Series II*, *86A*, 121–142. https://doi.org/10.2151/jmsj.86A.121

Tomita, H., & Satoh, M. (2004). A new dynamical framework of nonhydrostatic global model using the icosahedral grid. *Fluid Dynamics Research*, *34*(6), 357–400. https://doi.org/10.1016/j.fluiddyn.2004.03.003

Webb, M., Senior, C., Bony, S., & Morcrette, J.-J. (2001). Combining ERBE and ISCCP data to assess clouds in the Hadley Centre, ECMWF and LMD atmospheric climate models. *Climate Dynamics*, *17*(12), 905–922. https://doi.org/10.1007/s003820100157

Weisman, M. L., Skamarock, W. C., & Klemp, J. B. (1997). The resolution dependence of explicitly modeled convective systems. *Monthly Weather Review*, *125*(4), 527–548. https://doi.org/10.1175/1520-0493(1997)125<0527:TRDOEM>2.0.CO;2

Wyngaard, J. C. (2004). Toward numerical modeling in the "terra incognita". *Journal of the Atmospheric Sciences*, *61*(14), 1816–1826. https://doi.org/10.1175/1520-0469(2004)061<1816:TNMITT>2.0.CO;2

Yoneyama, K., Zhang, C., & Long, C. N. (2013). Tracking pulses of the Madden–Julian oscillation. *Bulletin of the American Meteorological Society*, *94*(12), 1871–1891. https://doi.org/10.1175/BAMS-D-12-00157.1

Yoshida, R., Nishizawa, S., Yashiro, H., Adachi, S. A., Sato, Y., Yamaura, T., & Tomita, H. (2017). CONeP: A cost-effective online nesting procedure for regional atmospheric models. *Parallel Computing*, *65*, 21–31. https://doi.org/10.1016/j.parco.2017.04.004